Comparison of deep-ocean finescale shear at two sites along the Mid-Atlantic Ridge

Timothy F. Duda
Applied Ocean Physics and Engineering Department
Woods Hole Oceanographic Institution
Woods Hole, Massachusetts, USA

October 3, 2005

Abstract

Four drifting floats were used to measure the magnitude of the vertical derivative of horizontal velocity in waters above the rough bathymetry of the Mid Atlantic Ridge. This derivative is typically the dominant component of the velocity gradient (the shear). Two floats were at the site of the Brazil Basin Tracer Release Experiment (BBTRE) in the South Atlantic, and two were near the site of the Guiana Abyssal Gyre Experiment (GAGE) in the North Atlantic. Floats operated for one year except for one BBTRE float which operated for 100 days. Shear was measured over a vertical span of 9.5 m using drag elements that caused the floats to rotate slowly in response to shear. For each float, the first, second and fourth moments of shear were elevated above levels associated with the Garrett-Munk model internal-wave spectrum. Three of the four floats were tracked as they moved over mountainous terrain, allowing shear intensity to be measured as a function of height above the bottom. A deep BBTRE float showed enhancement of rms shear near the bottom. Floats at both areas provided measurements at 2000 m above the bottom, with differing results: The GAGE site had a lower fourth moment of shear (diapycnal diffusivity proxy) than the BBTRE site. However, application of normalization factors accounting for differences between the sites in bottom roughness, latitude-dependent internal-wave dynamics, and tidal current speeds brings the results into agreement.

Keywords: Internal waves, internal wave shear, diapycnal mixing

1. Introduction

The process of internal wave generation by deflection of tidal currents above sloping bottoms has been the subject of accelerating interest over the last decade. One of the motivations for this has been uncertainty about the role of diapycnal mixing in meridional overturning circulation, and in other ocean circulation patterns (Munk and Wunsch, 1998; Wunsch and Ferrari, 2004). Internal wave conditions and diapycnal mixing influences on circulation have uncertain geographic distribution. Furthermore, on a site-by-site basis, the fraction of diapycnal mixing directly attributable to instability of tidally forced internal waves is poorly known.

The idea that flow interaction with the bottom, tidal flow or otherwise, leads to localized intense diapycnal mixing, and that the increased potential energy is communicated to the interior through isopycnal processes, has been investigated for a few decades (Armi, 1978; Ivey, 1987). Both boundary-layer and wave generation/radiation/instability processes have been considered. However, the vastness and diversity of the world's oceans have allowed only gradual progress in the field investigation of these interacting processes.

The recent Hawaii Ocean Mixing Experiment (HOME) was a targeted study of internal tides (tidally forced internal waves) and mixing at the dramatic Hawaiian Ridge feature of the North Pacific Ocean (Rudnick et al., 2003). HOME found large internal tides and intense mixing near the ridge, and found that internal wave energy and shear decreased with distance from the ridge. The Brazil Basin Tracer Release Experiment (BBTRE) measured dissipation and diffusion near the seafloor in a deep-water region of rough fracture zones and abyssal hills (Ledwell et al., 2000). BBTRE also measured microstructure in waters above an abyssal plain (Polzin et al., 1997). This experiment detected weak dissipation (implying weak diapycnal mixing) above the plain, and detected stronger dissipation and diffusion above the rough area. Other studies have found weak internal waves above regions of smooth seafloor (Kunze and Sanford, 1996), strong internal wave shear and/or strain above regions of rough seafloor (Naveira Garabato et al., 2004; Polzin, 1999), and density finestructure evidence for mixing above areas of rough seafloor (Mauritzen et al., 2002).

To provide additional field data applicable to the study of diapycnal abyssal mixing and internal waves in areas of rough seafloor, we have deployed floats to measure the small-amplitude internal-wave shear that is characteristic of deep ocean waters. This paper presents data from floats deployed in two locations of the Atlantic Ocean. An important feature of the data set is that one site shows more internal-wave shear at 2000 m above the bottom than does the other site. A second feature is that scaling the shear statistics with three normalization factors accounting for known differences between the sites brings the results from the two locations into closer agreement.

Both locations are on the western slope of the Mid-Atlantic Ridge, one at about 22 degrees south and one at about 13 degrees north (Fig. 1). The southern location is that of BBTRE. The northern location is the site of the Guiana Abyssal Gyre Experiment (GAGE), which used moorings and surveys to look for a northward recirculation of the deep western boundary current on the eastern side of Guiana Basin. In each region, two drifting floats were used to obtain time series of the magnitude of the vertical derivative of horizontal velocity (the shear). Samples were obtained in an integrating manner over one-hour intervals. Work of recent decades supports and quantifies the intuitive link between the intensity of internal-wave shear (specifically the fourth raw moment of shear, where the nth raw moment is the expected value of a random variable taken to the nth integral power) and turbulent diapycnal mixing (Gregg, 1989; Polzin, Toole and Schmitt, 1995). This means that our records of internal-wave activity can serve as a proxy for diapycnal diffusivity.

The methodology used here to estimate eddy diffusivity from internal wave shear assumes that diffusivity is proportional to the fourth moment of shear, with additional scaling factors that are functions of latitude and buoyancy frequency. For internal waves having the Garrett-Munk (GM) spectrum, the dissipation and diffusivity would be functions of only latitude. Departures from GM are observed, however, and result in variations in estimated eddy diffusivity that surpass the latitude effect.

Detailed results from the BBTRE floats have already been published (Duda, 2004). Some of the BBTRE float data are presented again here and compared with the more recently obtained GAGE float data. Our basic results are: (1) The intensity of shear exceeds that consistent with the Garrett-Munk internal wave model spectrum (Garrett and

Munk, 1972; Gregg, 1989; Gregg and Kunze, 1991; Munk, 1981); (2) At 1300-2300 meters above the bottom, the GAGE floats detected weaker shear than the BBTRE floats. (3) Multiplication by three scaling factors serving to account for three known differences between the GAGE and BBTRE sites brings the diffusivity results into concordance, suggesting a basic understanding of the role of the items which differ, which are tidal current speed, bottom roughness, and internal-wave dissipation processes.

The paper is organized as follows. Section 2 describes the shear data collection methods and the estimation of diapycnal mixing processes from the shear data. Section 3 presents data from the two sites. Section 4 presents shear fourth moments and implied mixing as a function of height above the bottom. Section 5 compares conditions at the two sites and applies scaling factors to account for differences between the two sites. In Section 6, the diffusivity estimates are compared with other field-derived values, and with values derived using computational modeling. Section 7 is a summary.

2. Data Collection and Data Analysis Methods

Shearmeter quasi-isobaric drifting floats were deployed at each of the two areas, BBTRE and GAGE respectively (Fig. 1). Two floats in each area returned long-term time series of hourly samples of shear magnitude S_h. The sampled quantity is the hour average, indicated with $\langle\rangle_h$, such that $S_h = \langle S\rangle_h = \langle \mid \mathbf{S} \mid\rangle_h = \langle \mid \mathbf{i}u_z + \mathbf{j}v_z \mid\rangle_h$. Instantaneous shear S is defined as

$$S = \left[\left(\frac{\Delta u}{\Delta z}\right)^2 + \left(\frac{\Delta v}{\Delta z}\right)^2\right]^{1/2} \tag{1}$$

where Δu and Δv are east and north velocity component differences taken over the vertical separation of $\Delta z = 9.5$ meters. The Shearmeters sense S directly once per second, not the components.

Measured shear (S_h) has a least-count value of 1.8×10^{-4} s^{-1} (equivalent to a 0.17 cm/s velocity difference over the 9.5-m span.) Fig. 2 shows a twenty-day portion of the shear time series from one of the floats. The solid line shows a low-pass filtered version of the hourly data, which are shown with a dotted line. Note that shear fluctuates strongly in space (and/or time), so that, assuming stationary statistics, long time series aid in computation of statistics such as the mean or higher moments. Details of float operations

appear in Duda (2004).

Parameterizations can be used to estimate diapycnal mixing effects from finescale shear measurements such as ours. Here, as in previous work (Duda, 2004; Duda and Jacobs, 1995), the expression of Gregg (1989) is used to estimate kinetic energy dissipation rate, which is one of the primary sources of energy for diapycnal mixing processes. This is based on theoretical behavior of internal waves of large vertical wavenumber propagating within a field of internal waves having the Garrett-Munk (GM) internal wave spectrum (Garrett and Munk, 1972; Garrett and Munk, 1975; Munk, 1981). The large-wavenumber waves refract and have evolving vertical wavenumber, intrinsic frequency, group velocity, energy density, etc, and are predicted to dissipate in a manner explained by Henyey, Wright and Flatté (1986). The expression is

$$\epsilon_G = 1.67\, C E^2 \pi^{-1} j_*^2 b^2 N^2 \left[f \cosh^{-1}(N/f) \right] R \tag{2}$$

where j_*, E, and b are parameters of the GM spectral model. Specifically, the mode bandwidth $j_* = 3$, the dimensionless energy level $E = 6.3 \times 10^{-5}$, the main-thermocline e-folding scale $b = 1300$ m, and $R = \langle S_{10}^4 \rangle / S_{GM}^4$ is the fourth moment of shear scaled by its value in the GM model. N is the buoyancy frequency and f is the Coriolis parameter. The quantity measured here and input to the expression is $\langle S_{10}^4 \rangle = \langle (2.11 S_h^2)^2 \rangle$, with the scaling of 2.11 explained in Gregg (1989). The calculation of the normalization factor S_{GM}^4, which is the fourth moment of shear in the GM model, and which is a function of f and N, is explained in Duda (2004). The empirical constant $C = 2$ is not part of GM.

Digressing for a moment, the GM wavenumber/frequency spectrum has separable wavenumber and frequency factors, has vertically symmetric wavenumber content, has horizontally isotropic wavenumber content, and has no special treatment of internal tides. The parameters j_*, E, and b of the model, and other parameters such as exponents, have been chosen so that the model fits a variety of ocean observations in a non-rigorous sense. The mode bandwidth j_* controls the shape of the vertical mode number (or vertical wavenumber) spectrum, and the scalar E scales the total energy.

Two important aspects of the scaling are the proportionality of ϵ_G and the fourth moment of shear from internal waves of vertical wavelengths exceeding 10 meters, $\langle S_{10}^4 \rangle$, and the proportionality of ϵ_G and N^2. There is a latitude (θ) dependence to the formula,

entering via f and shown in brackets, which has been examined (Gregg, Sanford and Winkel, 2003; Hibiya and Nagasawa, 2004). This term reflects a theoretical influence on the rate of wave breaking by the frequency content of the internal wave spectrum, which changes as the allowable bandwidth widens at decreasing latitude. This effect is examined in Section 5.1.

To apply the expression to the dataset, note that four parameters in the equation vary between floats and over time for a given float. These are N, f, and $\langle S_{10}^4 \rangle$, and S_{GM}^4. The other parameters are held fixed, as with other published applications of this relationship.

Because internal waves obeying GM are implicit in the use of (2), is it desirable for consistency that data be collected where the internal wave spectrum resembles GM. This somewhat confounds the usefulness of the expression in regions departing from GM, but we proceed in this manner nonetheless, as have others (e.g. Naveira Garabato et al. (2004)). A more complex expression intended to correct in a rudimentary way for effects of wavefields diverging from GM that involves finescale strain could also be used (Polzin, Toole and Schmitt, 1995), as was done by Naveira Garabato et al. (2004), but this is not possible for this data set because strain measurements from the floats had high noise levels. Note here that inapplicability of GM at very low latitudes is not a problem here (Levine, 2002).

Taking another step, diffusivity can be computed from dissipation (Gregg and Kunze, 1991; Osborn, 1980):

$$K_G \leq E \epsilon_G N^{-2} \tag{3}$$

The factor $E = R_{fc}/(1 - R_{fc})$ is a maximum mixing efficiency, with R_{fc} being the critical flux Richardson number (Ellison, 1957). Equality is generally assumed when this expression is used to estimate diffusivity, and this is done here, with a constant mixing efficiency $\Gamma = 0.2$ substituted in place of E. Arguments for Γ being in this vicinity are given in Osborn (1980). The validity of this expression, with equality and $\Gamma \sim 0.2$, has been supported by two concurrent tracer and dissipation profiling studies, the North Atlantic Tracer Release Experiment (Ledwell, Watson and Law, 1998; St. Laurent and Schmitt, 1999) and the Coastal Mixing and Optics Experiment (Ledwell et al., 2004; Oakey and Greenan, 2004).

Further details of how these expressions are applied to Shearmeter data can be

found in Duda (2004). Details of the BBTRE deployments such as deployment positions can be found in a report (Duda et al., 2002) and in a journal article (Duda, 2004). The GAGE float data are presented here for the first time. The two GAGE floats providing data for this paper were launched on 19 Feb 2001 from *RV Oceanus* within a few hundred meters of 13° N, 49° W.

3. Shear Data and Statistics

Data from two floats at each of the two sites are presented. Table 1 gives float serial numbers (SN), the temperatures and depths at which the floats sampled, and the water masses they were in. The floats drifted at pressures from 1660 to 3150 dbar, and at potential temperatures from 2.36 to 3.65°C. The floats were in either Upper, Middle, or Lower North Atlantic Deep Water (NADW) volumes, which are defined in Mauritzen et al. (2002). These classes of water originate from more dense bottom waters formed at high latitude in both polar regions (Luyten et al., 1993), and knowledge of flux into and out of these classes would provide important constraints on global circulation and ocean climate conditions. The long and awkward 7075 alloy Shearmeters were difficult to ballast in Woods Hole harbor because of tidal currents, and did not settle at the correct depths. Nonetheless, they successfully sampled the targeted NADW. (The widely ranging serial numbers reflect the fact that these first-generation Shearmeters were modified Seascan Inc. RAFOS floats with RAFOS controller serial numbers. The controller in Shearmeter 001 was a prototype and was subsequently used in RAFOS floats as well as Shearmeters.)

Data concerning float trajectories are shown in Table 2. Three of the floats were tracked for 365 days, while one float, shallow BBTRE float 001, drifted untracked for 100 days. Deep BBTRE float 100 moved eastward on to the Mid-Atlantic Ridge, Fig. 3. The shallow GAGE float (139) moved to the east northeast, Fig. 4, while the deep GAGE float (140) moved to the west northwest, consistent with the postulated Guiana Abyssal Gyre (M. McCartney, personal communication). The high rms velocities of the tracked floats (Table 2) and the looping trajectories indicate that the sample mean velocities are only rough indicators of longer-term mean velocities.

Figs. 5 and 6 show records of S_h^2 from the four floats. The squares show daily mean values of this quantity. The shaded areas are bounded by daily minima and maxima. The

data fluctuate in an apparently random manner. Variations at many time scales are evident, as expected. Statistics of the shear data are given in Table 3. The N values (unmeasured by us) are important for the comparison of shear moments to S_{GM} and for use of expressions (2) and (3). shear intensity and thus of predicted dissipation and diffusivity. These were obtained from Levitus database values (Levitus, 1982) and from pre-existing CTD casts in both experimental areas. In the ocean, N is a fluctuating quantity in both Lagrangian and Eulerian frames, so the CTD measurements are only indicators of the mean N encountered by the float. The stated N values are thought to be within 10% of the true mean values, based on analysis of fluctuations of a few profiles in each of the two experimental areas.

Gradient Richardson numbers computed from the ratio of the square of mean N to the mean squared S_h range from 0.44 to 0.73. The lowest value number is for BBTRE float 100, which displays the highest shear variance when scaled by the GM value, as well as the highest fourth moment of shear scaled against the GM value. The ratios of shear second moment to the squares of S_{GM} exceed unity by factors of four to six. The ratios of the fourth moments to S_{GM}^4 are also large. Departure from two of the ratio $\langle S_h^4 \rangle / \langle S_h^2 \rangle^2$ suggests that the components u_z and v_z from which S_h is derived are not joint normal (Gregg, 1989; Gregg and Kunze, 1991).

The values of the fourth-moment ratio R from the final column of Table 3 can be used to compute average dissipation and diffusivity values, which are listed in Table 4. The values in the final column also express the ratio of the estimated dissipation and diffusivity values to those that are consistent with the GM spectral model at the proper N and f (i.e. latitude) for each float. The K_G values are all higher than is consistent with GM because all R are greater than 1. R range from 11 to 16 except for the high value of 36 for the deep BBTRE float.

4. Shear vs. Height Above the Bottom

Direct comparison of shear moments (and of implied mixing via (2) and (3)) from different floats requires some care because the floats were at different heights above the bottom and at different depths. If shear is largely due to internal waves generated by flow/topography interaction and radiating upward, then these differences should be pertinent. The analysis can be done by examining subsets of shear data binned according to float height above the bottom, as was done in Duda (2004), instead of comparing statistics from the complete time series. This binning allows more detailed analysis of the data from each float, as well as better intercomparison between the floats.

The time series of height of each tracked float above the seafloor was computed directly using a bathymetric database (Smith and Sandwell, 1997). With this knowledge, the binning according to height above the bottom was accomplished, and statistics were computed within each bin. Using 400-m height bins, we computed R as a function of height above the bottom (h), giving $K_G(h)$ (Fig. 7). A point is included for untracked BBTRE float 001, which gave $K_G = 3.3 \times 10^{-5}$ m^2/s at ≈ 3000 m.a.b. The most notable feature of Fig. 7 is the discrepancy between the K_G values at heights above the bottom sampled by floats in both regions, namely 1300 to 2400 m above the seafloor. Further discussion of the BBTRE profile appears in Duda (2004).

5. Comparison of the Two Sites

In this section, the K_G determinations at positions 1300 to 2400 m above the bottom are examined. At these depths, the BBTRE K_G were between 0.67 and 0.91 cm^2/s, while the GAGE float 140 values ranged from 0.26 to 0.44 cm^2/s and the GAGE float 139 values were 0.27 and 0.34 cm^2/s. Thus, the GAGE values are 28 to 65 percent of the BBTRE values (approximately one-half).

Comparisons of internal tide predictions for various seafloor morphologies have been published. St. Laurent and Garrett (2002) compared internal tide generation and energy fluxes at the slow-spreading rough Mid-Atlantic Ridge and the fast-spreading smooth East Pacific Rise. St. Laurent and Nash (2004) compared internal tides at the Hawaiian Ridge with those of the Mid-Atlantic Ridge. The three morphologies of those studies have

distinct internal-tide generation tendencies and dynamics. In contrast, the situation here is more subtle because the differing GAGE and BBTRE shear records were all collected above physically similar portions of the Mid-Atlantic Ridge.

Here, we discuss five processes that could cause the observed differences at ∼2000 m.a.b. The first is the theorized latitude scaling of internal wave propagation and breaking which is implicit in (2). The second is possible seasonal variations of internal wave surface forcing. The remaining three are related to seafloor-generated internal waves. For these waves, created by the action of currents over sloping areas, it is possible that subtidal currents, seafloor roughness, and/or tidal currents may differ between the GAGE and BBTRE sites. This gives five possible explanations for the diversity of K_G values. Of these, three effects prove to be quantifiable in the five subsections to follow: The latitude, roughness, and tidal current effects.

5.1. Latitude

One important difference between the two sites is the latitude θ. This offers a possible explanation because $f = 2\omega \sin\theta$ appears in the numerator of expression (2), contributing to the GAGE K_G values being lower than the BBTRE values. ω is the rotation rate of the earth. The factor f arises in the expression because the Doppler shifting rate of small-scale (near dissipation) waves is a function of the aspect ratio of the dominant waves, and the dominant waves are usually near-inertial, with frequencies slightly greater than f (Gregg, Sanford and Winkel, 2003). This term has been examined with ocean data, and the case to support the latitude effect is strong. However, the effect of the term has not been examined in isolation from other geographically or temporally induced differences between data sets, so its veracity has not been completely confirmed. This effect can be accounted for in our data with normalization involving the quantity $F_i = f_i \cosh^{-1}(N_i/f_i)$ computed for each float, with the subscript i indicating float number, and with a standard value F_s equal to F_i computed for the deep GAGE float (140). The expression is

$$K_L = K_G(F_s/F_i) \tag{4}$$

The ratios F_s/F_i are 0.84, 0.57 and 0.71 for floats 139, 001, and 100, respectively.

If K_L values from the different regions were to agree, then the latitude effect alone

would explain the differences seen in Fig. 7. Multiplying the BBTRE deep float 100 K_G results at the depths of interest by 0.71 brings them closer to the GAGE values, but still in excess. Thus, the latitude scaling offers a partial explanation.

5.2. Seasonal Variation

There is a possibility of a seasonal effect, which would presumably be caused by seasonal variation of wind-forced internal waves propagating down from the surface. The selected (∼2000 m.a.b) BBTRE float 100 data are from the initial stages of the mission, during austral fall and winter. The selected GAGE data were taken year-round. Seasonal dependence of internal waves and mixing was observed in the North Atlantic Tracer Release Experiment at the shallow position of 300 dbar, at greater than 4000 m above the bottom (Duda and Jacobs, 1995; Ledwell, Watson and Law, 1998). In that experiment, the winter diapycnal mixing of tracer exceeded that of the summer by 50 percent, and spring internal wave shear exceeded that of fall. If winds generated a significant fraction of the BBTRE-site internal wave shear, then increased winter winds might explain the BBTRE excess K_G (or GAGE K_G deficit). There is no apparent seasonal signal in the BBTRE float 100 data. However the data are from a variety of depths, and there are no 2000 m.a.b. data from this float in the summer, so this effect cannot be ruled out.

5.3. Subtidal Currents

Subtidal currents flowing over seafloor features can generate gravity waves. Steady currents generate waves of known character (Gill, 1982). Nonsteady flow will cause transients in the upward wave energy flux. The BBTRE float came close to the bottom and was thus able to measure the flow very near the seafloor. Its drift indicates that subtidal and tidal current speeds were of comparable magnitude, so that each effect could have generated internal waves at that location (Duda, 2004). However, the GAGE floats were never close to bottom, so we do not have GAGE near-bottom subtidal speeds for comparison. The GAGE experiment moorings collected current records hundreds of km to the northwest of the GAGE float area, but this distance probably exceeds the correlation scale of the near-bottom subtidal flows. Thus, the relative importance of wave generation at the two sites by the action of subtidal near-bottom currents is an open question.

5.4. Seafloor Roughness Variability

The two sites have similar but not identical bathymetric detail. The differences may be responsible for differences in internal-wave fields generated by the action of either tidal or subtidal flow over the topography. The differences are not strong, however, so they are an unlikely total explanation for the differing estimated K_G values of the two sites at 1300-2400 m.a.b. The bathymetric differences may have caused an increase of BBTRE shear parameters above GAGE by up to 10 percent, based on analysis presented in the remainder of this section.

Figs. 8 and 9 show BBTRE-site and GAGE-site bathymetry taken from the Smith and Sandwell (1997) database. Statistics of depths along the tracks in the gridded regions of the figures are given in Table 5. The gridded regions are intended to be representative of regions occupied by the GAGE and BBTRE floats while they were 1300 to 2400 m.a.b (i.e. while they collected the data we are comparing here). The bathymetric character at the two sites is similar in many ways, which is not surprising since the sites are similar in distance from the spreading ridge, and are of similar age because the spreading rates are comparable.

To first order, physical properties of the seafloor are a function of age, with the lithosphere and asthenosphere cooling and subsiding with age (Parker and Oldenburg, 1973). The relative ages of the two sites can be seen in Figs. 8 and 9. Crustal isochrons 5, 6, 13 and 18 are shown. These represent ages of 9.6, 20.2, 33, and 40 million years, respectively. The GAGE gridded region has a mean age of about 33 million years, the BBTRE gridded region a mean age of 25 million years.

Table 5 gives seafloor parameters computed for the gridded subset regions. The greater mean depth at GAGE is consistent with the age difference. The older GAGE site also has slightly lower rms gradient and rms height variability, consistent with erosion. Overall, the slightly higher gradients and rms heights of the younger BBTRE site suggest a slightly increased capacity to generate internal tides or internal waves, offering a partial explanation for the increased reduced shear intensity at the BBTRE location.

To higher order, specific details of fault structures, mass wasting, and sedimentation can modify roughness at scales of 0.1 to 1000 cycles/km over time (Goff and Tucholke,

1997), and spatial variability of these processes can lead to heterogeneity of similarly aged crust, but there are no strong indications of highly different conditions at BBTRE and GAGE in the database. To investigate in slightly more detail, along-fracture zone and across-fracture zone power spectra computed using the gridded bathymetry are shown in Fig. 10. One-dimensional spectra of this type were employed by St. Laurent and Garrett (2002) in an investigation of internal-tide generation at two types of spreading ridges, slow-moving (like the Mid-Atlantic Ridge) and fast-moving. Alternatively, two-dimensional spectra could be shown. The spectra are similar but not identical. One difference between them is the barely-resolved shift in the cross-fracture zone spectral peak from 1.8×10^{-5} cyc/km (GAGE) to 2.2×10^{-5} cyc/m (BBTRE), which is a shift from 55 to 45 km scale. This should not affect internal wave generation. Another difference is the increased short-wavelength along-fracture zone variability in GAGE relative to BBTRE (red lines). Increased roughness at short wavelength may be expected to elevate GAGE internal waves, all else being equal, which is counter to the observation of less internal-wave shear at GAGE.

St. Laurent and Garrett (2002) demonstrate that the upward internal tide energy flux per unit of horizontal internal-wave wavenumber, as given by linear theory (Bell, 1975), is quite similar to the spectrum of bathymetric slope, although it tapers off faster with increased wavenumber. Furthermore, they give an expression for the Richardson number, showing it to be inversely related to a scaled version of the bathymetric spectrum. For a given N, this indicates that Richardson numbers should be inversely proportional to the bathymetric height variances given in Table 5, which are integrals of the spectra. It is sensible to assume that the height variances and the shear fourth moments would have a direct relationship, but the precise relationship is not possible to evaluate without making a number of perhaps unjustifiable assumptions. For this reason, we claim only that the slightly smoother GAGE bathymetry is consistent with the reduced shear intensity at 1300-2400 m above bottom at GAGE with respect to BBTRE. It is also consistent with the higher Richardson number for the GAGE floats than for the deep BBTRE float (Table 3).

In summary, subtle differences in bathymetric roughness at the two sites are discernible from available data. The data suggest that the GAGE area is slightly smoother than the BBTRE area. Thus, the roughness difference is a viable explanation for the

reduced shear fourth moment (i.e. K_G) at GAGE (Fig. 7). However, the bathymetric difference is slight, perhaps 10 percent (Table 5). The sensitivity of internal-wave shear moments to bottom slope or roughness would need to be high for this to offer a complete explanation.

5.5. Tidal Current Variability

Tidal currents at the two sites can be predicted from the TPXO global inverse tide model (Egbert, Bennett and Foreman, 1994). Table 6 gives constituent current parameters computed from the model for each of the two experimental areas. The global bathymetric grid of 256 by 512 points is used in the computation of current. Constituents are similar in amplitude at the two sites, so they do not offer a trivial explanation for the K_G difference depicted in Fig. 7.

To further investigate, tidal timeseries were synthesized using the program tidhar for the eight constituents listed in Table 6. Fig. 11 shows hodographs of spring and neap tide portions of currents predicted for April 2001 for the two sites, which are typical of spring and neap conditions. The motions are anticyclonic in each case. They have similar peak speeds at the two sites, about 4 cm/s. However, the mean current speeds computed for a few months at the two sites differ, 1.8 cm/s at GAGE versus 2.2 cm/s at BBTRE, as do the mean squared currents, 4.0 $(\mathrm{cm/s})^2$ at GAGE versus 5.5 $(\mathrm{cm/s})^2$ at BBTRE.

The ratio of mean-squared speeds at GAGE and BBTRE of 0.73 is noteworthy because the squared velocity appears in an expression for upward wave energy flux developed by Bell (1975) and recently used by St. Laurent and Garrett (2002). The expression is for the case of small tidal excursion with respect to the scale of the bathymetry, and for harmonic forcing. Departure from unity of the ratio of mean-squared speeds at the two sites therefore offers a third explanation for the lower shear fourth moments observed at GAGE, although the value of 0.73 is not as low as the estimated GAGE/BBTRE K_G ratio of about 0.5.

There are differences in the hodographs at the two sites that may be significant to the internal tide generation problem, and may further explain the decreased activity at GAGE. It can be seen in Fig. 11 that the tidal currents are quite different in nature at the two sites, being more rectilinear at GAGE than an M_2 internal wave ellipse (the tidal

currents at both sites are predominantly semidiurnal), but being more circular than an M_2 ellipse at BBTRE. A concordance between tidal current hodographs and internal wave hodographs might be expected to enable production of internal waves of different character than would a situation with non-concordant motion.

Note that temporal variability of shear at BBTRE shows only a weak correlation with fortnightly tidal modulation (Duda, 2004), suggesting that processes other than tides, such as subtidal currents (section 5.3), may play an important role in abyssal shear variability and mean value. These processes are less amenable to prediction than tidal processes, and their possible role tempers the value of the tidal correction.

5.6 Normalization of Results

Scaling $R(h)$ and $K_G(h)$ to account for the varied latitude, roughness, and tidal current speeds would allow better intercomparison of the results from each of the four floats. Recall that Fig. 7 shows a factor of two discrepancy between BBTRE and GAGE K_G curves.

Scaling the K_G (or ϵ_G) values by normalization factors that are similar to the F_i latitude factors of section 5.1, but instead related to seafloor roughness and tidal currents, in such as way as to bring them into agreement would suggest that these effects are indeed playing a role and that the role is understood. This analysis is performed here.

It is sensible to separate the latitude effect, which deals with flux of internal wave energy through the spectrum and with the dissipation of waves (section 5.1), from the roughness and tide effects, which presumably affect the generation of waves.

First, the effects of bottom roughness and tide current speeds on internal wave generation, and subsequently on the value of R are crudely accounted for. The roughness factors are called ζ_i and ζ_s, and the tidal current factors are called u_i and u_s, following the convention described in section 5.1. The deep GAGE float number 140 is taken as the standard, as with latitude normalization. The normalized shear is

$$R_N = R(\zeta_s/\zeta_i)(u_s/u_i) \tag{5}$$

with subscript i indicating float number and subscript s indicating standard, as in (4). For GAGE floats, ζ_s/ζ_i and u_s/u_i are unity. For BBTRE floats, $\zeta_s/\zeta_i = 0.95$, accounting for the

the 5 to 10 percent rougher bathymetry at the BBTRE site. For the BBTRE floats, $u_s/u_i = 0.73$, accounting for the higher tidal current amplitude at BBTRE with respect to GAGE.

Fig. 12 shows $R(h)$ at the top. These were used to compute the K_G values in Fig. 7. The shear fourth moment is seen to vary between 10 and 40 times the GM value. The normalized $R_N(h)$ are plotted in the lower panel of Fig. 12. The normalization of the BBTRE data to account for the increased BBTRE-site tide current speeds and roughness compared to those at the GAGE site bring the observed shear into better agreement.

Next, all three effects can be accounted by considering normalized diffusivity

$$K_N = K_G(F_s/F_i)(R_N/R) = K_G(F_s/F_i)(\zeta_s/\zeta_i)(u_s/u_i) \tag{6}$$

This is shown in Fig. 13. The product of the three correction factors is roughly 0.5 for the BBTRE floats. The K_N are seen to lie on a smooth curve and are in close agreement at the depths where data are available from more than one float.

The nonlinearity of internal-wave generation, propagation, and dissipation processes casts some doubt on the validity of this simple multiplication of scaling factors, but the result shown in Fig. 13 is intriguing.

6. Comparison with Measured and Modeled Diffusivity Values

It is useful to compare the numerical values of the diffusivity estimates shown in this paper (Table 4, Fig. 7) with those estimated from other field studies over similar terrain. There are many published numbers, and they have a broad range. The BBTRE tracer injection experiment provided a diapycnal diffusivity value of about $K = 3 \times 10^{-4}$ m^2/s at 4000 m depth, the heart of the tracer patch, with diffusivity increasing with depth to $K = 8 \times 10^{-4}$ m^2/s at 4500 m depth (Ledwell et al., 2000). Mountains in the area reached up to 4000 m depth, with valley floors as deep as 5000 m. The tracer did not disperse upward to positions above 3600 m depth, which is 400 to 1400 m above the bottom, and thus provided no mixing information there. These K values are three or more times greater than our maximum K_G value of 9×10^{-5} m^2/s. Dissipation measurements taken during BBTRE gave an estimate of $K = 2.3 \pm 1 \times 10^{-4}$ m^2/s at depths occupied by the patch (Ledwell et al., 2000). The lower bound of this is close to the values from the deeper

BBTRE float.

A paper that analyzes finescsale CTD transect data from the GAGE area suggests that K values above the Mid-Atlantic Ridge in the North Atlantic are 1 to 10×10^{-4} m^2/s (Mauritzen et al., 2002). The low range of these is about twice the K_G value reported here, but the discussion in that paper may be referring to positions closer to the bottom than where most of our data are from. The high range of these values exceed those reported here. That paper uses parameterizations like (2) and (3) except that the square of the strain spectral density is used there in place of shear to the fourth power.

The best direct comparison to make with this data set is against abyssal shear data collected with the geomagnetic induction method (Kunze and Sanford, 1996). Those data had mean shear variances of one to two times those of GM for all depths above a smooth plain, less than our values of four to six times GM above rough terrain (Table 3). Diapycnal diffusivity values given in that paper range from 0.6 to 6×10^{-5} m^2/s, with typical values lower than those reported here (Table 4, Fig. 7). That paper showed, with scant evidence, a tendency for near-bottom diffusivity to increase with near-bottom current speed.

A computational modeling paper suggests that 1 terawatt of dissipated tidal energy is converted to internal tidal energy (of 3.5 terawatts dissipated in the ocean), and that this is consistent with a global average diffusivity profile that ranges from 3×10^{-5} m^2/s in the thermocline to 7.7×10^{-4} m^2/s at depths, with a depth average of 9×10^{-5} m^2/s (Simmons et al., 2004). The depth average is equal to the largest of our values (Fig. 7). We have only limited data, so this is not inconsistent in a rigorous way, but the agreement is not good. That paper advocates a K profile starting at $K \sim 8 \times 10^{-4}$ m^2/s near the bottom at 5000 m depth, decreasing linearly to $K \sim 3 \times 10^{-5}$ m^2/s at 3000 m depth (2000 m above bottom), and holding near that value up to the surface. Another paper compares global circulation computed with a mixing profile having a topographic enhancement at the bottom (similar to that of Simmons et al. (2004)) with circulation computed with constant $K = 1 \times 10^{-5}$ m^2/s everywhere (Saenko and Merryfield, 2005). Alas, that work suggests that topographically enhanced mixing has little effect on Atlantic circulation, although it does suggest that topographically enhanced mixing affects the Pacific and Southern Oceans.

7. Summary

One-year long records of internal-wave shear were collected from four drifting floats in abyssal waters at two locations along the Mid-Atlantic Ridge. All records show similar temporal variability. The variability appears to be random, although statistical tests are not presented here, and probability density functions are not examined in detail. Probability density functions of $\langle S^4 \rangle$ for the year-long series (100 days for one float) resemble log-normal, but test show that the hypotheses that each data set is log-normal is to be rejected. The shear-squared data do not fit the rayleigh distribution, and the fourth moments are not twice the square of the second moments, indicating that the two shear components are non-gaussian. This is possibly due to data set nonhomogeneity, misunderstood sensor response, or both.

There are no strong seasonal dependencies in the data, although there are periods of elevated or reduced shear that last for periods of a few weeks to a month or more (Figs. 5 and 6). Statistical f tests show that variability between subsets of shear data in 10-day long windows are inconsistent with the subsets being merely different samplings of a single population, and that the variation at periods greater than about two weeks that is visible in the figures is in fact real (i.e. the degrees of freedom accumulate rapidly enough in the records to measure variation at those intermediate periods).

These float data have the advantage of sampling over periods that are long with respect to the time scales of observed variability and of fortnightly tidal interference. This reduces sampling uncertainty associated with the snapshot sampling of microstructure surveys (St. Laurent, Toole and Schmitt, 2001) and/or transects (Mauritzen et al., 2002). The BBTRE shear time series displays a hint of a corelation with the local barotropic tide (Duda, 2004). The shear to tide correlation at BBTRE is consistent with ability to collapse the shear data presented here onto a single line (Fig. 12) by considering the tide and the bottom roughness.

A float (100) close to the bottom at the BBTRE location in the South Atlantic measured higher shear moments than two floats at the GAGE location in the North Atlantic, and than a BBTRE float that was far from the bottom (Tables 3 and 4). Shear data from float 100 converts to an estimated diffusivity of order 1 cm^2/s. The other floats gave values near 0.3 cm^2/s, which is close to the value of ~ 0.15 cm^2/s that was measured in the main pycnocline (Ledwell, Watson and Law, 1998) and that is often cited.

The floats operated at different heights above rough topography, which is one probable source region for the internal waves that were present and were responsible for the shear. The different heights complicate direct comparison of data from different floats and regions. However, categorization of the data according to height above the bottom allows a better comparison. Three floats collected data at heights of 1300-2300 m above the bottom. At these heights, data from the BBTRE location possess higher shear fourth moment than data from the GAGE location. This is consistent with higher dissipation and diapycnal diffusion at BBTRE.

Three effects that may be responsible for the higher values of shear moments at the BBTRE site have been identified. These are: a latitude effect in wave propagation, refraction and breaking; slightly differing seafloor roughness at the two sites; and differing rms tidal current. Normalizing the BBTRE estimates with sub-unity scaling factors for each of these processes brings the two data sets into better agreement. No support is given for the simple multiplication of the scale factors, which implies a general linearity of the processes at work in determining the observed moments of internal-wave shear. Although these data do not comprehensively measure all aspects of the internal wave field, the agreement of the data from the various floats after the normalization process (Fig. 13) lends support to three hypotheses. First, the tidal current strength plays a role. Next, the magnitude of roughness is important. Third, the propagation, refraction and breaking physics, which the latitude correction is intended to account for, is correct. Note that the multiple processes at work in determining the shear field mean that the scaled measurements could agree after these corrections by chance or by accident, of course. This possibility must be considered until more abyssal internal wave data, dissipation data, and diffusion data are collected and used in studies of this type.

As a caveat, note that subtidal currents near the bottom at BBTRE were measured to have the same speeds as the tidal currents (Duda, 2004), so that the mesoscale currents may also interact with the bottom to generate internal waves. The data collapse onto similar curves (Fig. 13) despite disregarding this effect. (Mesoscale currents near the bottom were not measured by the GAGE floats, so a normalization using such currents is not possible.)

The shear data reported here stand independently of their interpretation as a

diffusivity proxy. Furthermore, the differences between data sets collected at the different sites have provided evidence that topographically produced internal waves play a role in the ocean shear field, and probably also in the distribution of diapycnal mixing. On the other hand, the diffusivity values reported here are very limited. Comparing these precise values with global mean estimates, with regional values installed into circulation models, or with values obtained from the field using other means is only a beginning. The collection of more data of many types would shed light on the processes at work.

Acknowledgments

The support of James Ledwell and John Toole allowed the BBTRE data collection. The support of Mike McCartney enabled the GAGE float project. Thanks are due to Webb Research Corporation and Seascan Inc. for float development and manufacture. The good ideas shared by the journal reviewers helped to improve the paper. This work was funded by the National Science Foundation under grants OCE9416014 and OCE9906685. This is WHOI Contribution 11403.

References

Armi, L., 1978. Some evidence for boundary mixing in the deep ocean. Journal of Geophysical Research 83, 1971–1979.

Bell, T. H. J., 1975. Topographically generated internal waves in the open ocean. Journal of Geophysical Research 80, 320–327.

Duda, T. F., 2004. Finescale shear at 1660 and 2850 dbar over the Mid-Atlantic Ridge in the eastern Brazil Basin. Journal of Physical Oceanogrphy 34, 1281–1292.

Duda, T. F., B. J. Guest, C. M. Wooding, C. M. Jones, S. Lelievre and D. C. Webb, 2002. Shearmeter floats in the area of the WHOI Brazil Basin Tracer Release Experiment: Technical and oceanographic data. Woods Hole Oceanographic Institution, WHOI Tech. Report WHOI-2002-01, Woods Hole, MA.

Duda, T. F. and D. C. Jacobs, 1995. Comparison of shear measurements and mixing predictions with a direct observation of diapycnal mixing in the Atlantic thermocline. Journal of Geophysical Research 100, 13,481–13,498.

Egbert, G. D., A. F. Bennett and M. G. G. Foreman, 1994. TOPEX/POSEIDON tides estimated using a global inverse model. Journal of Geophysical Research 99, 24,821–24,852.

Ellison, T. H., 1957. Turbulent transport of heat and momentum from an infinite rough plane. Journal of Fluid Mechanics 2, 456–4666.

Garrett, C. and W. Munk, 1972. Space-time scales of internal waves. Geophysical Fluid Dynamics 2, 225–264.

Garrett, C. J. R. and W. H. Munk, 1975. Space-time scales of internal waves: A progress report. Journal of Geophysical Research 80, 291–297.

Gill, A. E., 1982. *Atmosphere-Ocean Dynamics*. Academic Press.

Goff, J. A. and B. E. Tucholke, 1997. Multiscale spectral analysis of bathymetry on the flank of the Mid-Atlantic Ridge: Modification of the seafloor by mass wasting and sedimentation. Journal of Geophysical Research 102, 15,447–15,462.

Gregg, M. C., 1989. Scaling turbulent dissipation in the thermocline. Journal of Geophysical Research 94, 9686–9698.

Gregg, M. C. and E. Kunze, 1991. Shear and strain in Santa Monica Basin. Journal of Geophysical Research 96, 16,709–16,719.

Gregg, M. C., T. B. Sanford and D. P. Winkel, 2003. Reduced mixing from the breaking of internal waves in equatorial waters. Nature 422, 513–515.

Henyey, F. S., J. Wright and S. M. Flatté, 1986. Energy and action flux through the internal wave field: An eikonal approach. Journal of Geophysical Research 91, 8487–8495.

Hibiya, T. and M. Nagasawa, 2004. Latitudinal dependence of diapycnal diffusivity in the thermocline estimated using a finescale parameterization. Geophysical Research Letters 31, No. L01301.

Ivey, G. N., 1987. The role of boundary mixing in the deep ocean. Journal of Geophysical Research 92, 11,873–11,878.

Kunze, E. and T. B. Sanford, 1996. Abyssal mixing: Where it is not. Journal of Physical Oceanography 26, 2286–2296.

Ledwell, J. R., T. F. Duda, M. A. Sundermeyer and H. E. Seim, 2004. Mixing in a coastal environment: 1. A view from dye dispersion. Journal of Geophysical Research 109, C00013, doi:10.1029 / 2003JC002194.

Ledwell, J. R., E. T. Montgomery, K. L. Polzin, L. C. St. Laurent, R. W. Schmitt and J. M. Toole, 2000. Evidence for enhanced mixing over rough topography in the abyssal ocean. Nature 403, 179–182.

Ledwell, J. R., A. J. Watson and C. S. Law, 1998. Mixing of a tracer in the pycnocline. Journal of Geophysical Research 103, 21,499–21,529.

Levine, M., 2002. A modification of the Garrett-Munk internal wave spectrum. Journal of Physical Oceanography 32, 3166–3181.

Levitus, S., 1982. A Climatological Atlas of the World Ocean. NOAA Prof. Pap. 13, Princeton, NJ.

Luyten, J., M. McCartney, H. Stommel, R. Dickson and E. Gmitrowicz, 1993. On the sources of North Atlantic Deep Water. Journal of Physical Oceanography 23, 1885–1892.

Mauritzen, C., K. L. Polzin, M. S. McCartney, R. C. Millard and D. E. West-Mack, 2002. Evidence in hydrography and density fine structure for enhanced vertical mixing over the Mid-Atlantic Ridge in the western Atlantic. Journal of Geophysical Research 107, 3147, doi:10.1029/2001JC001114.

Muller, R. D., W. R. Roest, J. Y. Royer, L. M. Gahagan and J. G. Sclater, 1997. Digital isochrons of the world's ocean floor. Journal of Geophysical Research 102, 3211–3214.

Munk, W. and C. Wunsch, 1998. Abyssal recipes II: energetics of tidal and wind mixing. Deep-Sea Research I 45, 1977–2010.

Munk, W. H., 1981. Internal waves and small-scale processes. *Evolution of Physical Oceanography, Scientific Surveys in Honor of Henry Stommel*, B. A. Warren and C. Wunsch, Eds., MIT Press, 264–291.

Naveira Garabato, A. C., K. L. Polzin, B. A. King, K. J. Heywood and M. Visbeck, 2004. Widespread intense turbulent mixing in the southern ocean. Science 303 , 210–213 [DOI: 10.1126/science.1090929] .

Oakey, N. S. and B. J. W. Greenan, 2004. Mixing in a coastal environment: 2. A view from microstructure measurements. Journal of Geophysical Research 109, C10014, doi:10.1029 / 2003JC002193.

Osborn, T. R., 1980. Estimates of the local rate of vertical diffusion from dissipation measurements. Journal of Physical Oceanography 10, 83–89.

Parker, R. L. and D. W. Oldenburg, 1973. Thermal model of ocean ridges. Nature 242, 137–139.

Polzin, K., 1999. A rough recipe for the energy balance of quasi-steady internal lee waves. *Proc. 'Aha Huliko'a Hawaiian Winter Workshop*, 117–128.

Polzin, K. L., J. M. Toole, J. R. Ledwell and R. W. Schmitt, 1997. Spatial variability of turbulent mixing in the abyssal ocean. Science 276, 93–96.

Polzin, K. L., J. M. Toole and R. W. Schmitt, 1995. Finescale parameterizations of turbulent dissipation. Journal of Physical Oceanogrphy. 25, 306–328.

Rudnick, D. L., T. J. Boyd, R. E. Brainard, G. S. Carter, G. D. Egbert, M. C. Gregg, P. E. Holloway, J. M. Klymak, E. Kunze, C. M. Lee, M. D. Levine, D. S. Luther, J. P. Martin, M. A. Merrifield, J. N. Moum, J. D. Nash, R. Pinkel, L. Rainville and T. B. Sanford, 2003. From tides to mixing along the Hawaiian ridge . Science 301, 355–357.

Saenko, O. A. and W. J. Merryfield, 2005. On the effect of topographically enhanced mixing on the global general circulation. Journal of Physical Oceanography 35, 826–834.

Simmons, H. L., S. R. Jayne, L. C. St. Laurent and A. J. Weaver, 2004. Tidally driven mixing in a numerical model of the ocean general circulation. Ocean Modelling 6, 245–263.

Smith, W. H. F. and D. T. Sandwell, 1997. Global seafloor topography from satellite altimetry and ship depth soundings. Science 277, 1957–1962.

St. Laurent, L. and C. Garrett, 2002. The role of internal tides in mixing the deep ocean. Journal of Physical Oceanography 32, 2882–2899.

St. Laurent, L. and R. W. Schmitt, 1999. The contribution of salt fingers to vertical mixing in the North Atlantic Tracer Release Experiment. Journal of Physical Oceanography 29, 1404–1424.

St. Laurent, L., J. M. Toole and R. W. Schmitt, 2001. Buoyancy forcing by turbulence above rough topography in the abyssal Brazil Basin. Journal of Physical Oceanography 31, 3476–3495.

St. Laurent, L. C. and J. D. Nash, 2004. An examination of the radiative and dissipative properties of deep ocean internal tides. Deep-Sea Research II 51, 3029–3042.

Wunsch, C. and R. Ferrari, 2004. Vertical mixing, energy, and the general circulation of the oceans. Annuual Review of Fluid Mechanics 36, 281–314.

Figure Legends

Fig. 1. The two experimental sites are depicted with Shearmeter float trajectories. The GAGE site is in the North Atlantic near 13°N, 50°W. The BBTRE site is in the South Atlantic near 21°S, 17°W. Both sites are on the west side of the Mid-Atlantic Ridge. The blue and red lines at the GAGE site are two float tracks which are also shown in Fig. 4. The blue line at the BBTRE site is the track of the deep float whose data are shown in this paper. This track is also shown in Fig. 3.

Fig. 2. A portion of the record of hourly shear from GAGE float 139 is shown. Day zero is at the beginning of the record. The ill effects of a few missing System-ARGOS data packets on the raw and low-passed versions of the time series can be seen at days 100 and 104. Each packet contains data from a six-hour interval.

Fig. 3. The BBTRE deep float (number 100) trajectory is shown. The locations where the float was between 1600 and 2000 m above the bottom are shown in red. The locations where the float was between 2000 and 2400 m above the bottom are shown in light blue. The bathymetry is from Smith and Sandwell (1997).

Fig. 4. The trajectories of the two GAGE floats are shown. The trajectory of float 140 at 3150 dbar is at the left in blue, and that of float 139 at 1850 dbar is at the right in red. The floats were deployed together in time at the same location. The bathymetry is from Smith and Sandwell (1997).

Fig. 5. Shear squared from BBTRE floats 001 and 100 is shown. The squares show daily average values. The upper and lower edges of the gray areas show daily minima and maxima.

Fig. 6. Shear squared results from GAGE floats 139 and 140 are shown. The squares show daily average values. The upper and lower edges of the gray areas show daily minima and maxima.

Fig. 7. K_G values computed from data subsets binned according to height above the bottom are shown for three floats (100, 139 and 140). K_G is proportional to $\langle S_h^4 \rangle$ for each

curve. BBTRE float number 001 was not tracked, but was probably always above 2500 meters above the bottom, although it may have passed above a mountain rising to 2000 m below its depth that lies between the deployment and surfacing locations. The horizontal bars indicate the approximate rms error of each mean K_G value, based on the rms error of each mean $\langle S_h^4 \rangle$ estimate. These are the larger of the two error bars shown in this paper, the others being the bootstrap method error bars in Fig. 12.

Fig. 8. The Smith and Sandwell (1997) bathymetry data in the BBTRE area are s hown. The colored lines indicate a 2-d grid rotated with respect to lat./long. onto which depths are interpolated in order to compute the cross-fracture zone and along-fracture zone bathymetric spectra shown in Fig. 10. Crustal age isochrons from Muller et al. (1997) are shown in white.

Fig. 9. Similar to the previous figure except bathymetry data and isochrons in the GAGE area are shown.

Fig. 10. The spectra of bathymetry in along-fracture zone and across-fracture zone directions are shown.

Fig. 11. Tidal current hodographs synthesized for the two sites using the parameters of Table 6 are shown at the left. Two short records for April 2001 are plotted for each site, consisting of 31 hour samplings at spring and neap tides. At the right, semidiurnal internal wave hodographs are shown for the approximate BBTRE and GAGE latitudes, to be compared with the tide hodographs to the left of each.

Fig. 12. (upper panel) The shear fourth moment ratio $R = \langle S_{10}^4 \rangle / S_{GM}^4$ is plotted as a function of height above the bottom. The symbols show the mean values. The horizontal lines show 95% confidence intervals computed using the bootstrap method (500 iterations). The labels indicate the float number for each data curve (data point in the case of float 001). (lower panel) The normalized ratio values R_N computed from the data of the upper panel are shown. The normalization is non-unity only for BBTRE floats 100 and 001, and it scales the data downward to account for the effects of higher amplitude tides and increased roughness at the BBTRE site.

Fig. 13. Diffusivity vs. height above the bottom is shown, as in Fig. 7. However, diffusivity has been normalized as in (6). The GAGE/140 results of that figure are repeated (scale factor equal to 1). The GAGE/139 results are adjusted downward to reflect the minor effect of $\cosh^{-1}(N/f)$ discussed in section 5.1, because N is different for the two GAGE floats. The BBTRE results of Fig. 7 are scaled downward with three factors, accounting for $f\cosh^{-1}(N/f)$, the rougher BBTRE seafloor, and the stronger BBTRE tidal currents.

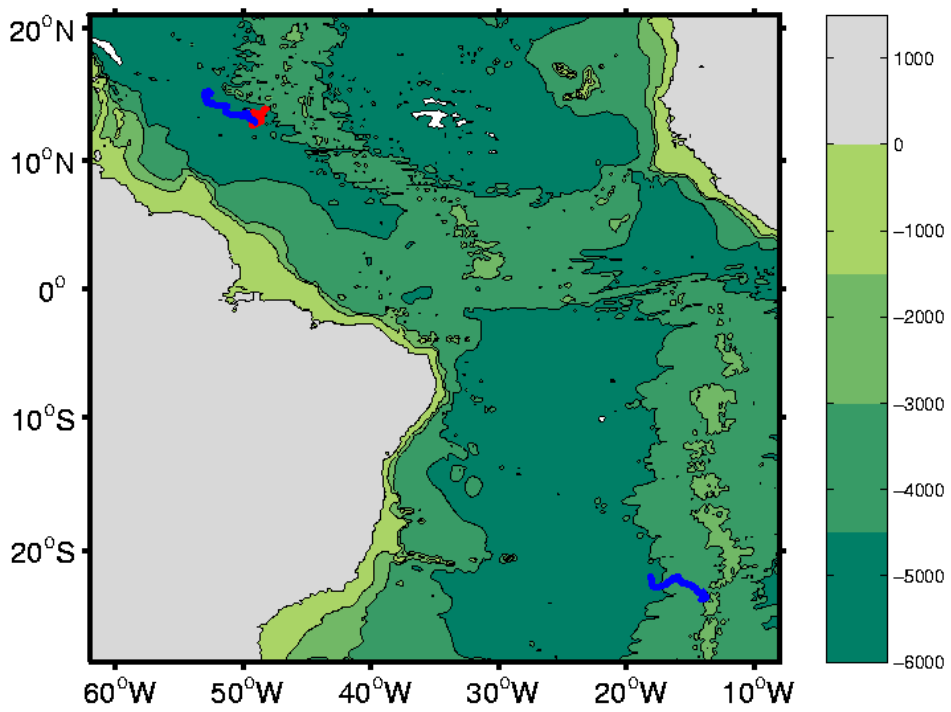

Figure 1: The two experimental sites are depicted with Shearmeter float trajectories. The GAGE site is in the North Atlantic near 13°N, 50°W. The BBTRE site is in the South Atlantic near 21°S, 17°W. Both sites are on the west side of the Mid-Atlantic Ridge. The blue and red lines at the GAGE site are two float tracks which are also shown in Fig. 4. The blue line at the BBTRE site is the track of the deep float whose data are shown in this paper. This track is also shown in Fig. 3.

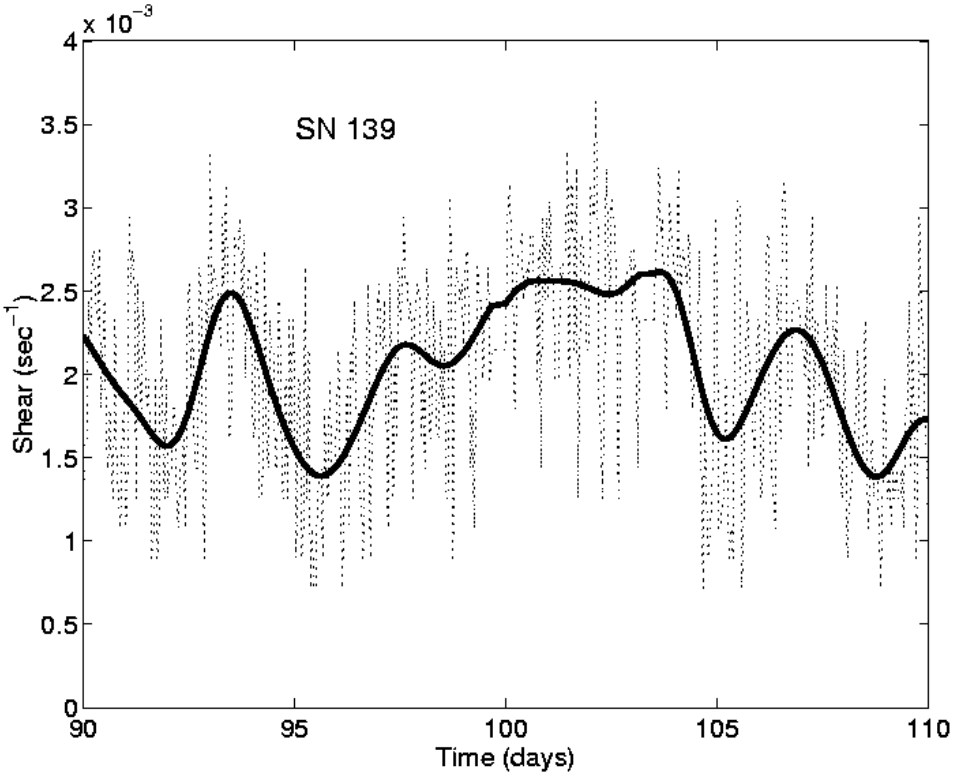

Figure 2: A portion of the record of hourly shear from GAGE float 139 is shown. Day zero is at the beginning of the record. The ill effects of a few missing System-ARGOS data packets on the raw and low-passed versions of the time series can be seen at days 100 and 104. Each packet contains data from a six-hour interval.

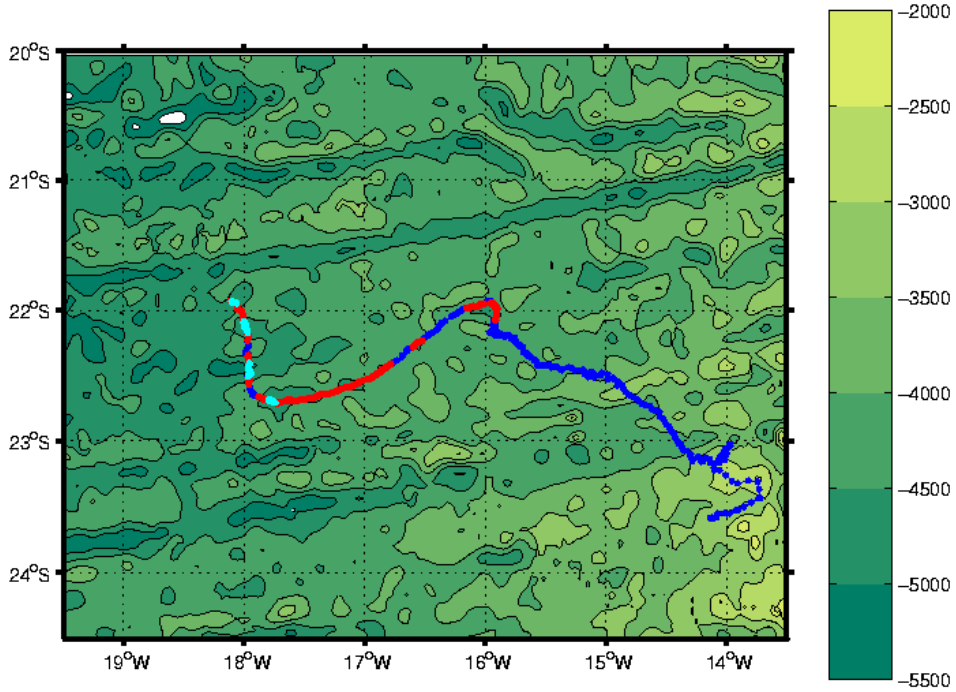

Figure 3: The BBTRE deep float (number 100) trajectory is shown. The locations where the float was between 1600 and 2000 m above the bottom are shown in red. The locations where the float was between 2000 and 2400 m above the bottom are shown in light blue. The bathymetry is from Smith and Sandwell (1997).

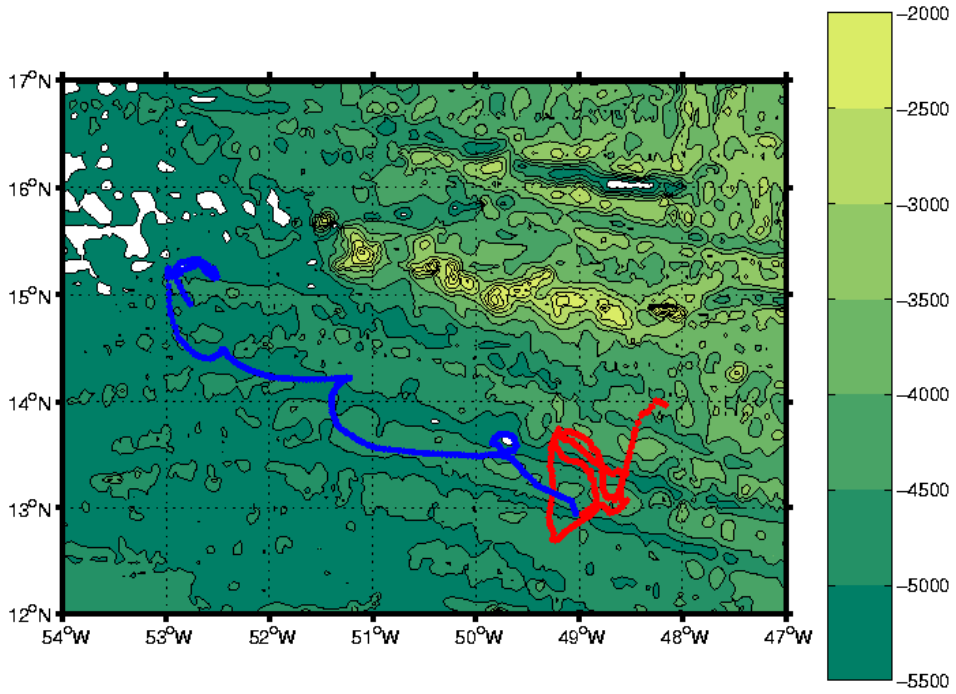

Figure 4: The trajectories of the two GAGE floats are shown. The trajectory of float 140 at 3150 dbar is at the left in blue, and that of float 139 at 1850 dbar is at the right in red. The floats were deployed together in time at the same location. The bathymetry is from Smith and Sandwell (1997).

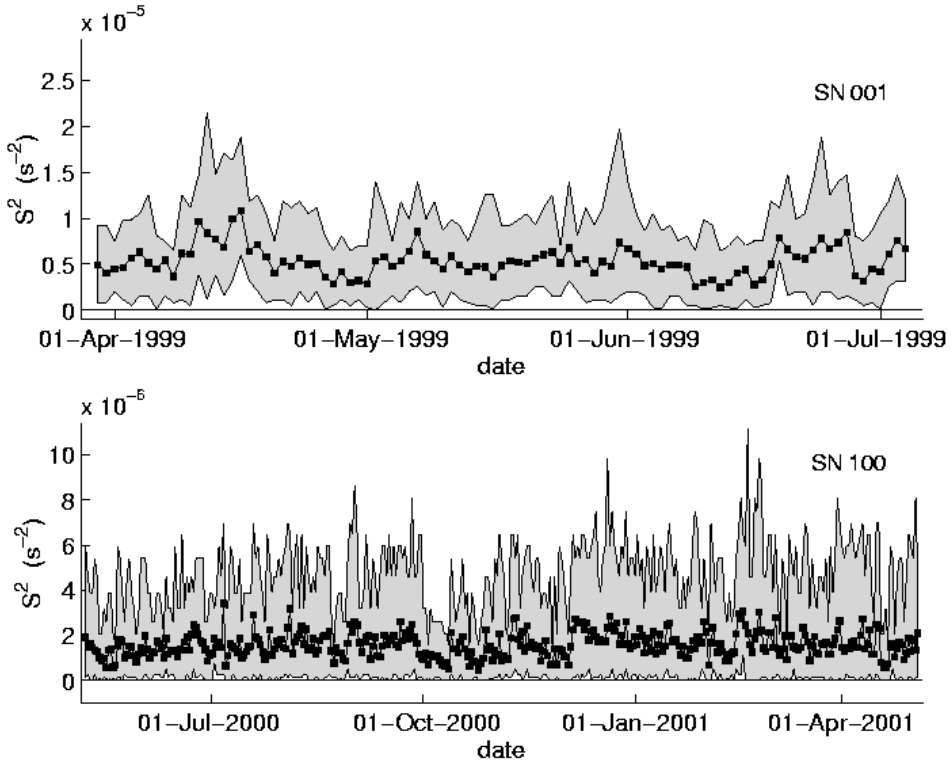

Figure 5: Shear squared from BBTRE floats 001 and 100 is shown. The squares show daily average values. The upper and lower edges of the gray areas show daily minima and maxima.

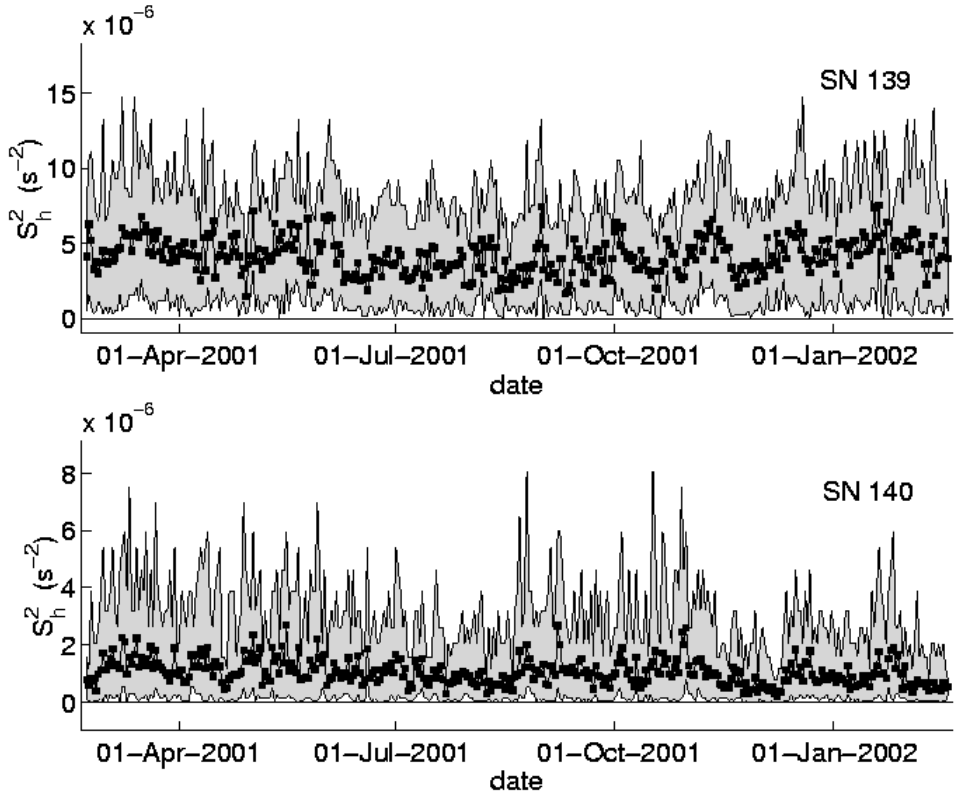

Figure 6: Shear squared results from GAGE floats 139 and 140 are shown. The squares show daily average values. The upper and lower edges of the gray areas show daily minima and maxima.

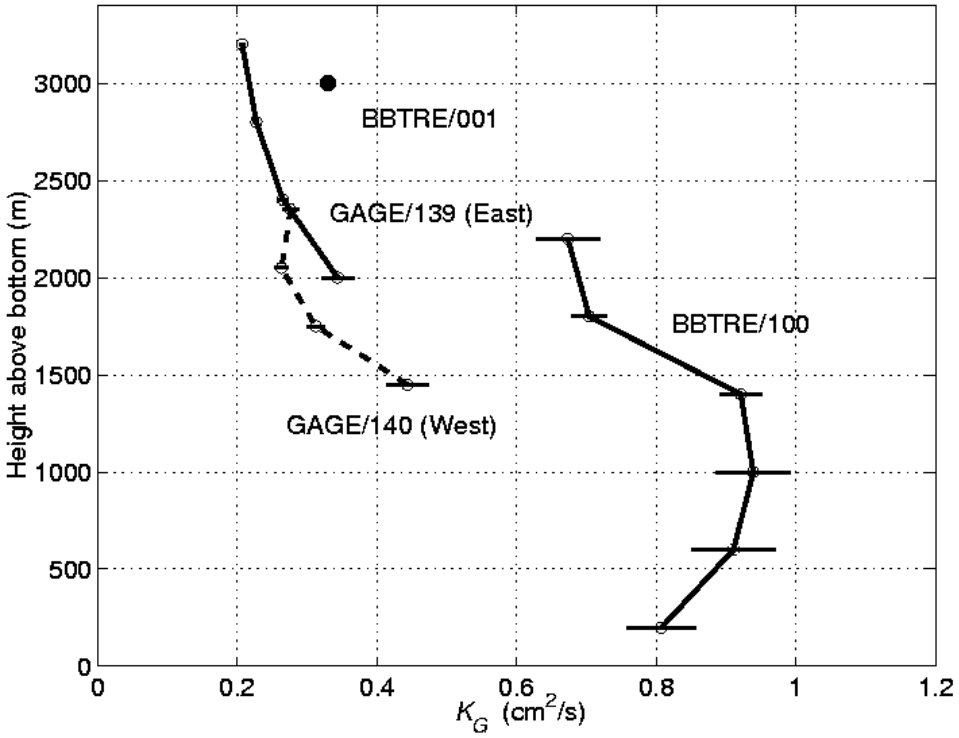

Figure 7: K_G values computed from data subsets binned according to height above the bottom are shown for three floats (100, 139 and 140). K_G is proportional to $\langle S_h^4 \rangle$ for each curve. BBTRE float number 001 was not tracked, but was probably always above 2500 meters above the bottom, although it may have passed above a mountain rising to 2000 m below its depth that lies between the deployment and surfacing locations. The horizontal bars indicate the approximate rms error of each mean K_G value, based on the rms error of each mean $\langle S_h^4 \rangle$ estimate. These are the larger of the two error bars shown in this paper, the others being the bootstrap method error bars in Fig. 12.

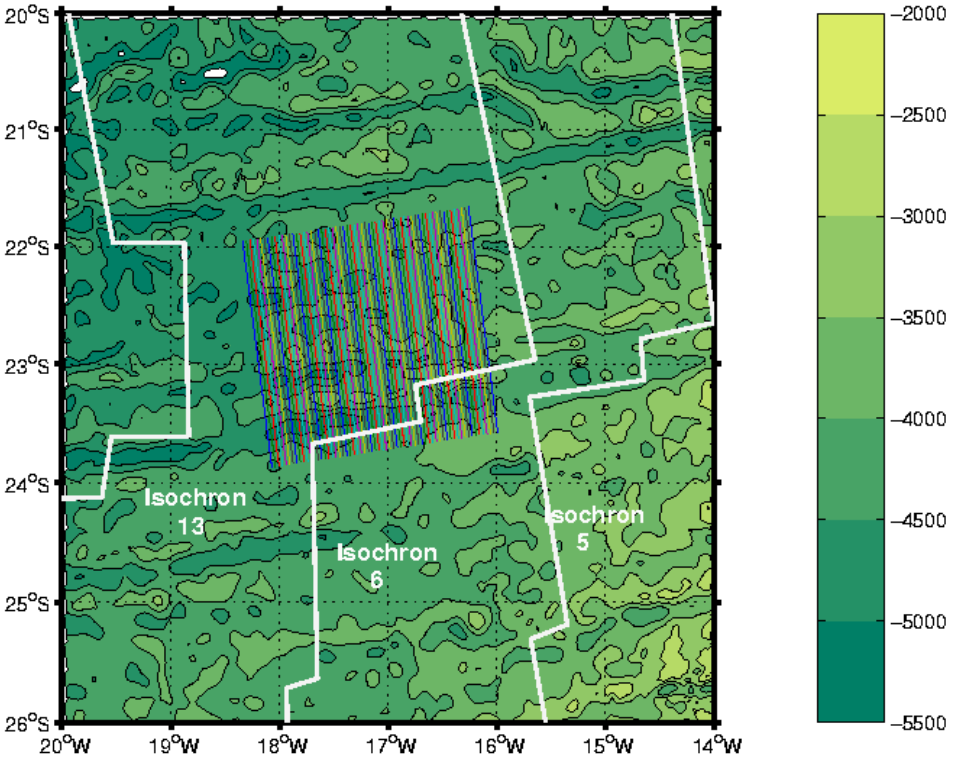

Figure 8: The Smith and Sandwell (1997) bathymetry data in the BBTRE area are shown. The colored lines indicate a 2-d grid rotated with respect to lat./long. onto which depths are interpolated in order to compute the cross-fracture zone and along-fracture zone bathymetric spectra shown in Fig. 10. Crustal age isochrons from Muller et al. (1997) are shown in white.

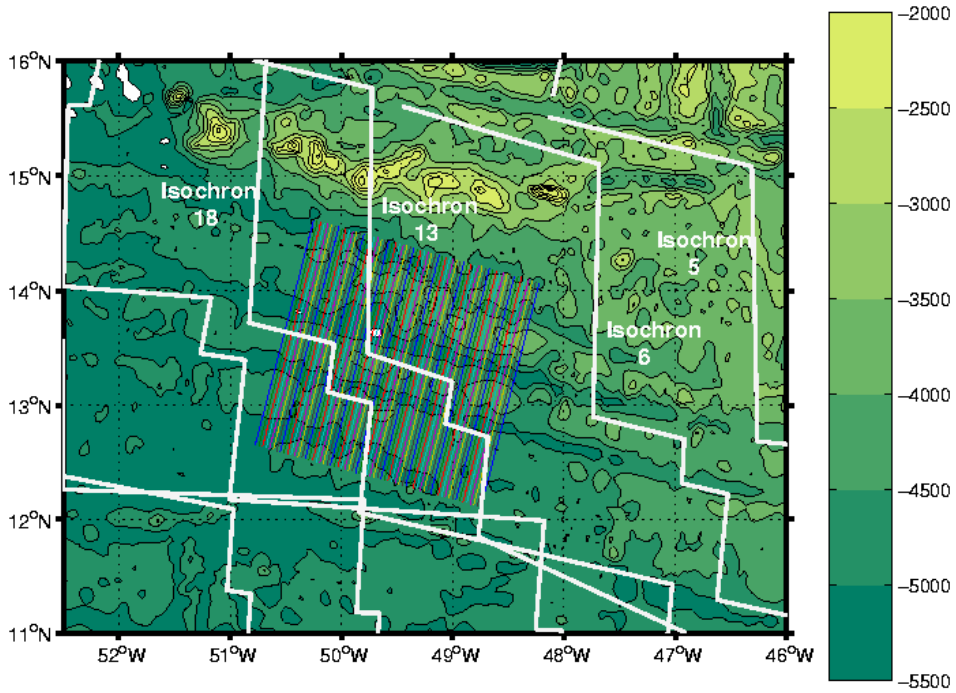

Figure 9: Similar to the previous figure except bathymetry data and isochrons in the GAGE area are shown.

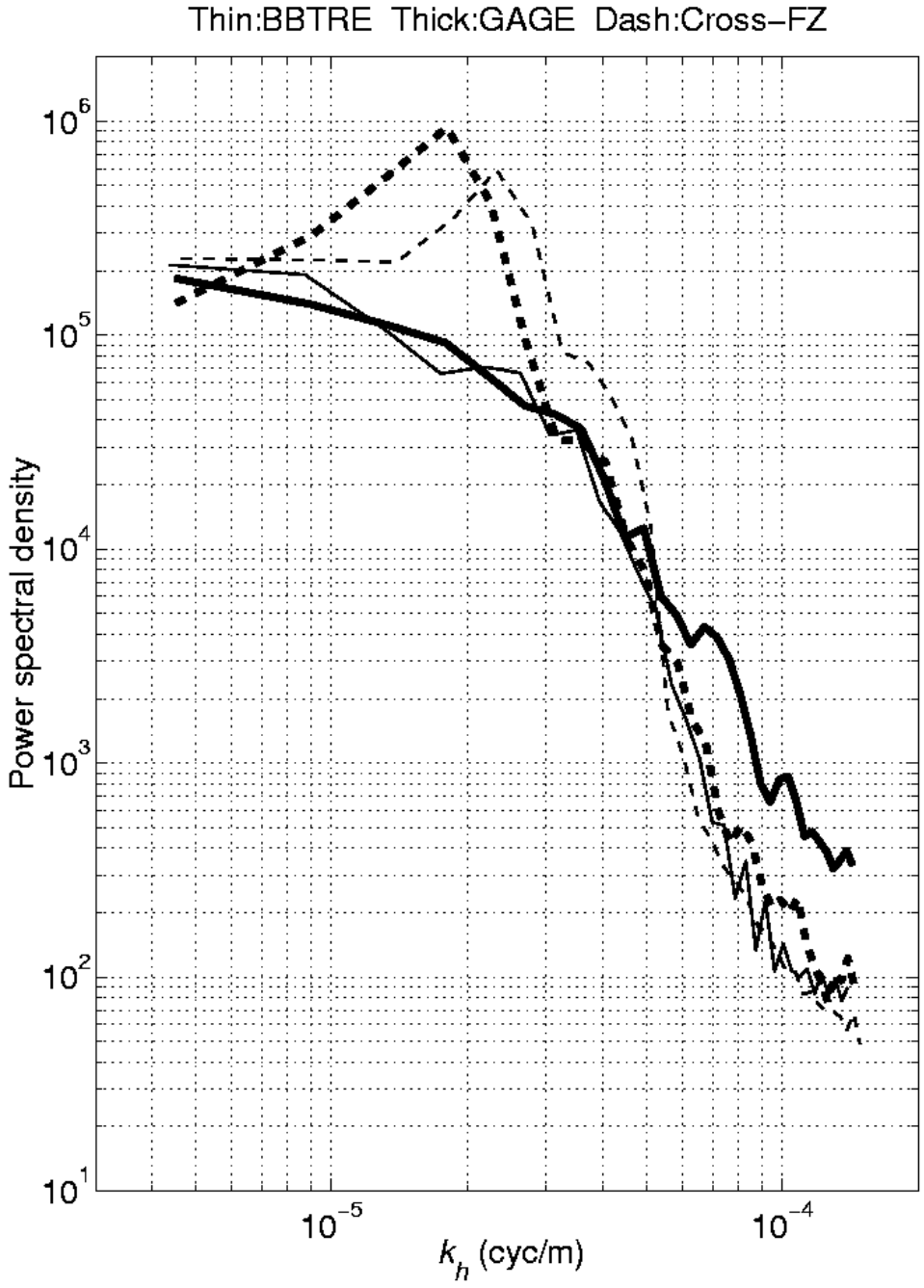

Figure 10: The spectra of bathymetry in along-fracture zone and across-fracture zone directions are shown.

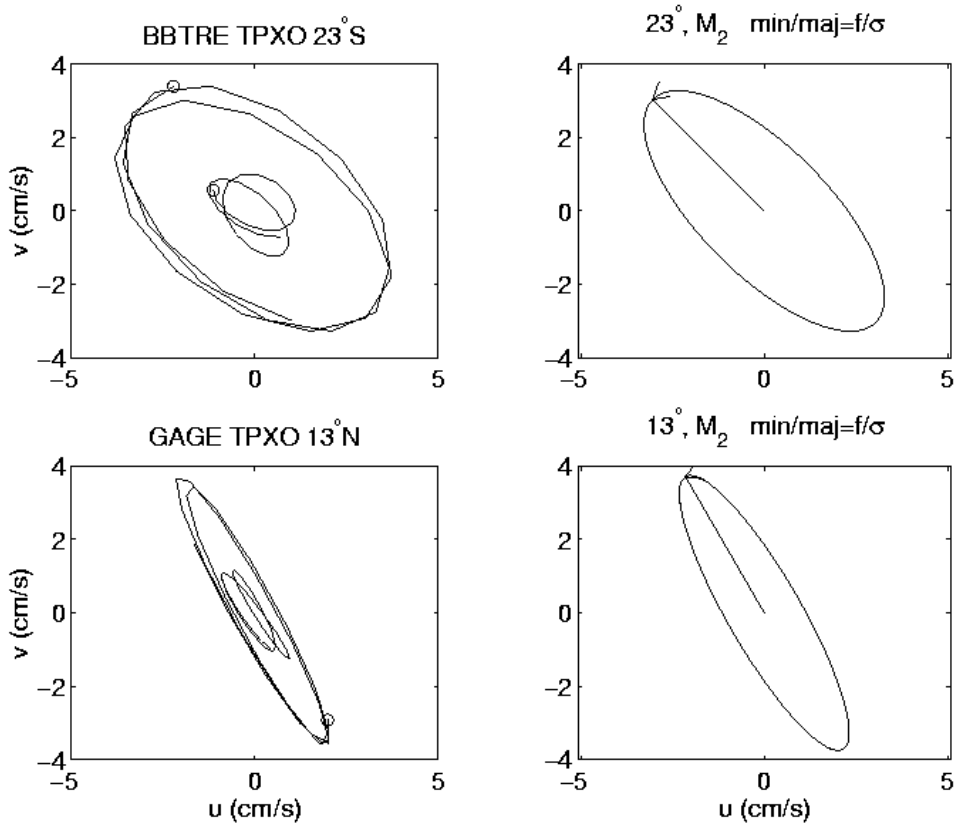

Figure 11: Tidal current hodographs synthesized for the two sites using the parameters of Table 6 are shown at the left. Two short records for April 2001 are plotted for each site, consisting of 31 hour samplings at spring and neap tides. At the right, semidiurnal internal wave hodographs are shown for the approximate BBTRE and GAGE latitudes, to be compared with the tide hodographs to the left of each.

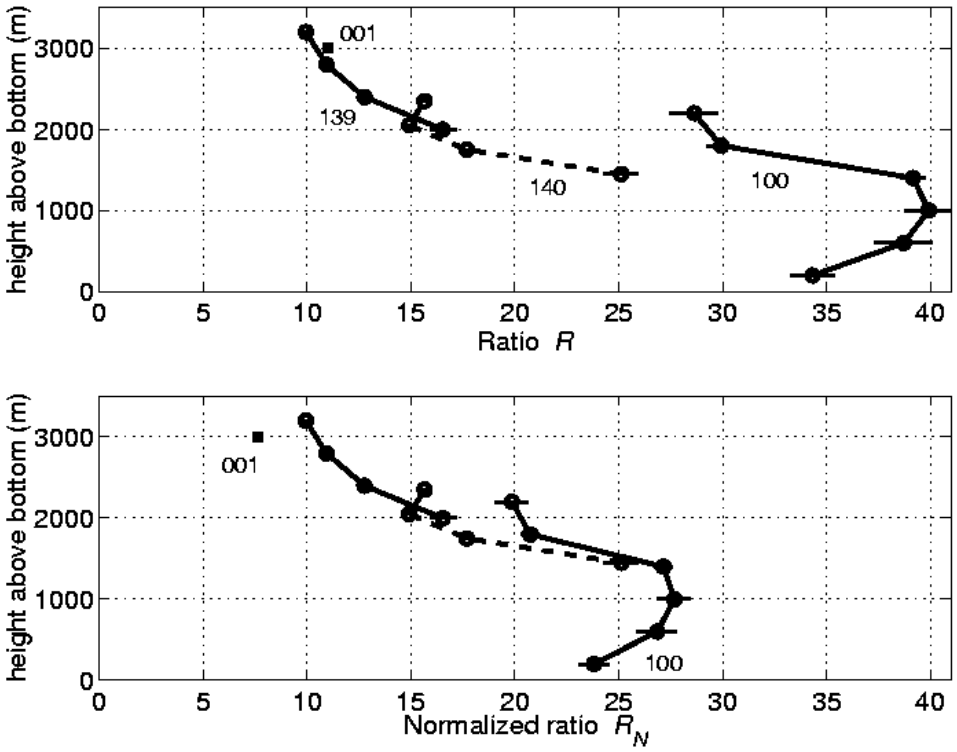

Figure 12: (upper panel) The shear fourth moment ratio $R = \langle S_{10}^4 \rangle / S_{GM}^4$ is plotted as a function of height above the bottom. The symbols show the mean values. The horizontal lines show 95% confidence intervals computed using the bootstrap method (500 iterations). The labels indicate the float number for each data curve (data point in the case of float 001). (lower panel) The normalized ratio values R_N computed from the data of the upper panel are shown. The normalization is non-unity only for BBTRE floats 100 and 001, and it scales the data downward to account for the effects of higher amplitude tides and increased roughness at the BBTRE site.

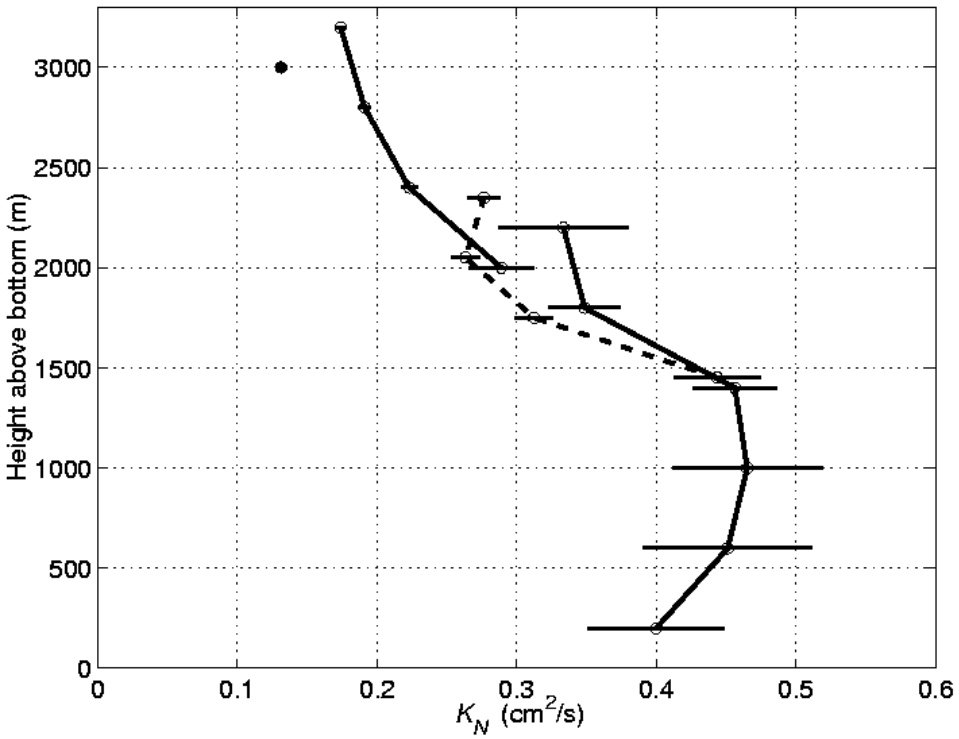

Figure 13: Diffusivity vs. height above the bottom is shown, as in Fig. 7. However, diffusivity has been normalized as in (6). The GAGE/140 results of that figure are repeated (scale factor equal to 1). The GAGE/139 results are adjusted downward to reflect the minor effect of $\cosh^{-1}(N/f)$ discussed in section 5.1, because N is different for the two GAGE floats. The BBTRE results of Fig. 7 are scaled downward with three factors, accounting for $f\cosh^{-1}(N/f)$, the rougher BBTRE seafloor, and the stronger BBTRE tidal currents.

Table 1. Float ballasting and water-mass sampling parameters.

Experiment	Float SN	Target ballasting	Actual sampling	Sampled pot. temp.	Water mass
BBTRE	001	2.9°C @ 1500 db	3.5°C @ 1660 db	3.37°	Upper NADW
BBTRE	100	1.8°C @ 3000 db	2.7°C @ 2850 db	2.50°	Middle NADW
GAGE	139	2.7°C @ 3000 db	3.8°C @ 1850 db	3.65°	Upper NADW
GAGE	140	2.5°C @ 3500 db	2.6°C @ 3150 db	2.35°	Lower NADW

Table 2. Table of float drift parameters. Speeds are listed in cm/s. Float 001 was not tracked and the data indicated with * are from deployment and surfacing positions.

Expt.	SN	Initial date	# days	Pres. (db)	Speed	Course	Rms u'	Rms v'
BBTRE	001	26 Mar 1998	100	1660	*1.43	*59°	–	–
BBTRE	100	6 May 2000	365	2850	1.28	117°	1.92	1.65
GAGE	139	20 Feb 2001	365	1850	0.55	74°	1.51	2.30
GAGE	140	20 Feb 2001	365	3150	1.03	277°	2.27	1.98

Table 3. Table of measured shear moments and related parameters. The moments are computed over the entire length of each record. Confidence intervals computed using the distribution of bootstrap resampled estimates of the moments vary among the floats. They are ±1.3% or less for the mean (first moment), ±2.2% or less for the mean square (second moment), and ±4.5% or less for the fourth moment.

Expt./SN	dbar	N (cph)	N^2	$\langle S_h \rangle$	$\langle S_h^2 \rangle$	$\langle S_{10}^2 \rangle / S_{GM}^2$	$\langle S_h^4 \rangle$	$R = \langle S_{10}^4 \rangle / S_{GM}^4$
BBTRE/001	1660	1.1	3.7×10^{-6}	2.2×10^{-3}	5.4×10^{-6}	4.1	3.8×10^{-11}	11
BBTRE/100	2850	0.5	0.7×10^{-6}	1.1×10^{-3}	1.6×10^{-6}	6.4	4.5×10^{-12}	36
GAGE/139	1850	1.0	3.0×10^{-6}	1.9×10^{-3}	4.1×10^{-6}	4.1	2.3×10^{-11}	11
GAGE/140	3150	0.5	0.7×10^{-6}	9.3×10^{-4}	1.1×10^{-6}	4.2	2.0×10^{-12}	16

Table 4. Table of implied dissipation and diffusion values. The computations are made using the the shear fourth moments computed over the entirety of each record.

Expt./SN	dbar	N (cph)	ϵ_G (W/kg)	K_G (m^2/s)
BBTRE/001	1660	1.1	6.1×10^{-10}	3.3×10^{-5}
BBTRE/100	2850	0.5	2.9×10^{-10}	8.3×10^{-5}
GAGE/139	1850	1.0	3.6×10^{-10}	2.4×10^{-5}
GAGE/140	3150	0.5	1.0×10^{-10}	2.8×10^{-5}

Table 5. Seafloor parameters. The data are for depths on grids with approx. 3 km spacing, shown in Figs. 8 and 9.

Site	Mean depth	Depth standard deviation	Rms gradient
BBTRE	4333 m	336 m	20.3 m/km
GAGE	4738 m	306 m	18.7 m/km

Table 6. Tidal constituent amplitudes and phases from TPXO. The chosen BBTRE location is 22° S, 18° W. The chosen GAGE location is 13.5° N, 50° W. Amplitude h is listed in cm/s, Greenwich phase g in degrees.

Constituent	BBTRE h	BBTRE g	GAGE h	GAGE g
u M_2	2.2986	-38.5372	1.3306	109.2970
u S_2	0.8568	-21.5704	0.3587	128.6848
u N_2	0.4837	-43.2491	0.2887	94.3500
u K_2	0.2293	-27.9843	0.0941	129.0879
u K_1	0.1203	-104.9376	0.2807	-63.3254
u O_1	0.1125	-179.4907	0.1284	-54.6023
u P_1	0.0368	-112.8714	0.0882	-62.8251
u Q_1	0.0248	141.0517	0.0152	-25.3821
v M_2	1.9880	79.7895	2.2699	-52.8115
v S_2	0.7108	97.6399	0.7379	-30.9345
v N_2	0.4510	68.9607	0.4840	-68.5129
v K_2	0.1878	93.4184	0.1975	-31.3966
v K_1	0.1691	167.3279	0.1769	91.3932
v O_1	0.3058	133.5692	0.0357	129.8877
v P_1	0.0606	161.4155	0.0527	91.3044
v Q_1	0.0762	109.6235	0.0180	-166.8142